Adhesion Properties of Swollen Hydrogels Evaluated by a Point-Contact Method

Atsushi Suzuki,[1] Takaya Sato,[1] Daisuke Sakasegawa,[1] Hidenori Sawada,[2] Motoaki Goto[2]

[1]*Faculty of Environment and Information Sciences, Yokohama National University, Yokohama 240-8501, Japan*
[2]*Saitama Daiichi Pharmaceutical Company Limited, Kasukabe, Saitama 344-0057, Japan*

Received 4 January 2007; accepted 6 March 2007
DOI 10.1002/app.26434
Published online 11 June 2007 in Wiley InterScience (www.interscience.wiley.com).

ABSTRACT: The adhesion of swollen hydrogels was studied with the use of a simple tack-evaluation technique using a point contact in the air at room temperature. The hydrogels used here were poly(sodium acrylate) gel physically crosslinked by aluminum ions. The adhesion properties were examined under different experimental parameters, i.e., separation velocities, normal loads, and waiting periods prior to separation. The effects of the material parameters resulting from the different degrees of the crosslinking on the adhesive properties were also examined. As a result, the adhesion force and the separation energy showed a power-law behavior with different powers, which depended on the experimental and material parameters. The adhesion properties were determined by the bulk viscoelasticity as well as the surface physical and chemical properties. The results were discussed in terms of the surface molecular interaction and the bulk viscoelastic and viscous properties on the basis of the measurements of the apparent contact area, the ATR FTIR spectrum, and the dynamic viscoelasticity. © 2007 Wiley Periodicals, Inc. J Appl Polym Sci 105: 3728–3738, 2007

Key words: adhesion of hydrogels; adhesion force; separation energy; FTIR; viscoelasticity

INTRODUCTION

The adhesion of the surfaces of soft materials is often an important factor when designing the performance, function, and reliability of commercial products. For example, the surface of an anti-inflammatory analgesic cataplasm should adhere firmly to the human body but not to the surface of another cataplasm. Many other products of soft materials, such as adhesive labels and tapes, have similar requirements. To improve the adhesion properties of the surfaces of soft materials, it is necessary to understand the mechanisms of bond formation and debonding separation of two soft materials. The physical and chemical properties of surfaces (such as the surface structure, molecular interaction, and viscoelastic properties) are essential factors in determining the adhesion properties of soft materials.[1–3]

Although the measurements of adhesion strength and energy by macroscopic methods are well established,[4–6] experimental techniques,[7–9] such as the peel test, the rolling ball test, and the probe tack test, often have a number of advantages and disadvantages depending on the experimental conditions as well as the material parameters. Recently we developed a new technique (a ''point-contact method'') for measuring the surface adhesion of soft materials,[10] in which the adhesion force, F_A, of a point contact of soft materials and the total energy, E_A, required to completely separate the contact can be easily and reproducibly obtained using the springs of phosphor-bronze thin plates with strain gauges (four active gauges). In this technique, two swollen hydrogels that were adhered on cylindrical glass sticks were placed in a crossed-cylinder geometry, thus, forming a point contact. Using this technique, it is relatively easy to obtain the dynamic adhesion properties characterized by two quantities of F_A and E_A with considerably high accuracy and reproducibility. The F_A between two soft materials can be defined as the maximum tension force during the connection that the adhesion can withstand before separation occurs. The E_A is dissipated throughout the separation process depending on the material parameters.

Among many contact mechanical models proposed in the literature,[11–17] the adhesion force between smooth (semi-) spheres or between a smooth (semi-) sphere and a smooth flat surface is a fundamental problem, which has been treated both analytically and experimentally on the basis of contact mechanical models, such as the Hertz, JKR, and

Correspondence to: A. Suzuki (suzuki@post.me.ynu.ac.jp).
Contract grant sponsor: Ministry of Education, Science, Sports and Culture in Japan, Kanagawa Academy of Science and Technology (KAST).

DMT methods. In a typical JKR test,[12] the work of adhesion is measured quantitatively using a single spherical material brought into contact with an opposing flat substrate through a loading and unloading cycle. The point-contact method[10] is very similar to numerous methods, including surface force apparatus, probe-tack measurements, which have been used over the last several decades to investigate the adhesion of soft materials or polymers. A crossed-cylinder geometry of the present experiment is mathematically equivalent to sphere on flat surface contact.[15] To understand the swollen gel-gel adhesion,[10] this specific experimental geometry of a point contact was used to minimize the effects of the interface boundary conditions to prevent the network structure from breaking. The curvature of cylinder is obtained by a clamp of thin plate gel on a cylindrical glass stick; it is not necessary to prepare the gels in a spherical or a cylindrical shape. This is one of the advantages to use this technique for the fragile soft materials, such as swollen hydrogels. Moreover, the sample preparation is very easy in the present method; the gel with a constant thickness is only adhered onto a glass stick. Therefore, the curvature as well as the thickness of gel can be arbitrarily selected by adjusting the diameter of glass stick and the gel thickness. This is another advantage of the present method. An essential uniqueness of the point-contact method has been proved by the following noteworthy fact[10]; the easiness to separate (rank of adhesion force and the separation energy) of seven anti-inflammatory analgesic cataplasms on the market by the use of this apparatus was consistent with the results of those obtained by organoleptic evaluations. Although the common mechanism between the present mechanical evaluation and the human senses have not been completely understood until now, it is possible to use universally the present technique to examine the adhesive performance of soft materials without relying on organoleptic evaluations.

Within our knowledge, there is a report on the swollen gel–gel adhesion[18] but in general it has not been extensively studied until now since the gel is fragile and it is difficult to conduct the mechanical experiments. In this article, the adhesion properties of a hydrogel were investigated by the point-contact method to prevent the difficulties to measure. The hydrogels used here were poly(sodium acrylate) hydrogels physically crosslinked by aluminum ions,[19,20] which have been widely used in the medical fields, such as an anti-inflammatory analgesic cataplasm. The main purpose of this article is to discuss the influence of the intrinsic (material) and extrinsic (experimental) parameters on the adhesion properties, in connection with the interfacial adhesion (surface physical and chemical properties) and the bulk elastic properties. Attenuated total refraction (ATR) FT-IR and dynamic viscoelastic measurements were conducted for several swollen gels with different degrees of crosslinking densities at room temperature.

EXPERIMENTAL

Sample preparation

Poly(sodium acrylate) gels, i.e., physically crosslinked polyelectrolyte hydrogels, were made of poly (sodium acrylate) and aluminum ions.[18,19] The pregel solution was obtained by mixing poly(sodium acrylate) (PSA) aqueous solution (for the main constituent, Wako, Chemical Industries, Japan) with aluminum hydroxide $Al(OH)_3$ (for the crosslinker, Kyowa Chemical Industry, Japan) of five concentrations, i.e., 1, 1.5, 2, 2.5, 3, and 4 wt %, of PSA solutions under acidic conditions. Each respective gel is designated here as ''PSA-Al(x) gel (x = 1, 1.5, 2, 2.5, 3, 4).'' The pregel solution was mixed with a spatula and sealed using Parafilm to prevent evaporation. Although the molecular weight of PSA should affect the gelation process, the PSA aqueous solution used here was a commercial reagent without further purification and the average degree of polymerization ranges from 2700 to 7500. The gel was shaped into a thin plate, which was prepared with the use of two flat plates (made of a glass slide and a polystyrene plate) and a 1-mm-thick spacer. A nonwoven textile with 0.6 mm thickness was attached with Scotch tape onto the slide. The mixed solution was mounted onto the nonwoven textile on the glass slide and sandwiched by the polystyrene plate, which was separated from the glass slide with the spacer. The solution on a set of flat plates was left in the air at room temperature (around 25°C) for 1 week. After gelation, the polystyrene plate was carefully removed from the gel by hand, thus forming a clamped thin plate gel on the upper surface of the nonwoven textile. Since the gel did not stick to the polystyrene plate, the gel surfaces were smooth macroscopically without crack, scratch and any other damage. The lower surface of the textile was adhered onto a glass stick with an 8-mm outer diameter using glue, resulting in the formation of a clamped thin plate gel on the glass stick. The top surface of gel has a curvature of a 5.6-mm radius. As-prepared gel can change its size (thickness) just after it was removed from the mold, even if all processes were conducted in the air (where water could not come out from or goes into the gel). This might result from the different degrees of crosslink and the different degrees of dehydration during gelation (7 days), which depended on the different amounts of $Al(OH)_3$. However, the maximum deviation of the

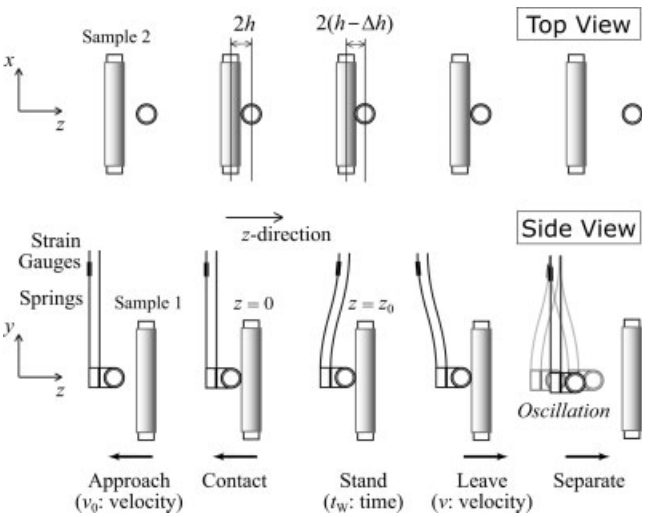

Figure 1 Schematics of the (a) top and (b) side views of the experimental setup and the method of measurement with 4 active strain gauges. z_0 was defined as the distance between the initial contact position and the final position of the position-controlled stage, and Δh was defined as the maximum length of the surface dent by the deformation of the respective sample.

sample thickness that we measured prior to adhesion testing was less than 5%, which corresponded to 1% for the curvature, R. In addition to the initial thickness change, the thickness may change during the measurements due to the dehydration. In the present experiment, the thickness change due to the dehydration was typically 5% (1% for the curvature, R) during the measurements (usually within 1 h).

In the PSA-Al(1) gel prepared with 1 wt % of $Al(OH)_3$, the molar ratio of sodium acrylate monomer units to Al ions was more than 15; therefore, the maximum amount of $Al(OH)_3$ contributing to the crosslinking was larger than 5 wt % of the PSA solution when the valence per Al ion is ideal, i.e., 3. Therefore, the degree of crosslinking was expected to increase with x ($1 \leq x \leq 4$), indicating that it was an important material parameter to determine the present samples.

Measurements of the adhesion force and separation energy

The contact area is formed by placing two glass sticks with the gels in a crossed-cylinder geometry (Fig. 1). One of the sticks (vertical in this figure; Sample 1; $x = z = 0$) was fixed to the position-controlled stage by the stepping motor and moved with velocity, v, in the range between 0.2 and 10 mm/s. The other stick (horizontal; Sample 2; $y = z = 0$) was fixed to the springs (a phosphor-bronze thin plate with dimensions of $0.1 \times 5.0 \times 30$ mm^3) with strain gauges (Kyowa, Electronic Instruments, Japan, KFG-2-120-C1-16 L1M2R). By moving Sample 1 with a constant advancing velocity, $v = v_0$ along the z-direction, Sample 1 could approach and contact Sample 2. By stopping the appropriate position, z_0, from the initial contact position (Fig. 1), the normal load, W, was initially adjusted using the calibration curve of the spring. However, W decreased during the approach with $v = v_0$ and slightly decreased for the waiting period, t_w, due to the relaxation of the deformation of gels caused by the contact. It is noteworthy that the total recovered distance by the relaxation was twice the deformation, Δh of the respective sample. After the position-controlled stage stopped and stood for t_w, it moved at a constant velocity, v, along the $+z$-direction (opposite to the approach) to completely separate Sample 1 from Sample 2. The strain gauge responded with a linear change in electrical resistance, which was calibrated using a set of well-known loads. We used four active gauges to maintain the accuracy of the measurements. The present measurements were conducted in the air at room temperature, and v_0 was fixed to 1.0 mm/s. The typical distance of the total movement of the position-controlled stage from the initial contact position, z_0, was 0.832 mm, which was small enough compared with the length of the spring.

Adhesion curve

A typical example of the relationship between the adhesion force, F, and the time, t, is shown in Figure 2. This adhesion curve consists of three processes; (1) the advancing contact of Sample 2 with a constant velocity, v_0 (from P_1 to P_2), (2) the standing at a

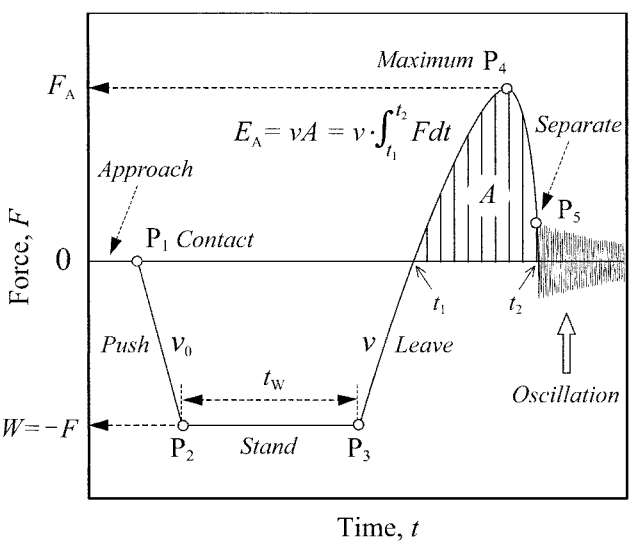

Figure 2 Schematic illustration of the adhesion curve, where A denotes the hatched area by vertical lines in this F-t plot. F_A and E_A were defined as the maximum F and the product of A and v (equal to the separation energy), respectively. After the separation, F quickly decreased to 0 with an oscillation.

constant position for a waiting period, t_w (from P_2 to P_3), and (3) the receding separation with a constant velocity, v (from P_3). After reaching the maximum at P_4, F rapidly decreased, and Sample 1 completely separated from Sample 2 at P_5. In this figure, F_A and E_A are defined, and W is the normal force (equal to $-F$). It is noteworthy that W slightly decreased (F increased) with t due to the stress relaxation brought about by the deformation of gels (see the next section). After complete separation, the gel oscillated for a while and attenuated in a few to several tens of seconds. The oscillation, however, could evidently not be observed in the case of a small x, where F gradually decreased to zero without an oscillation. In the following experiments, the position of the position-controlled stage for the standing was fixed to $z_0 = 0.832$ mm, which produced a 10 gf restoring force by the present spring distortion.

Although the absolute values of F_A and E_A slightly depended on the samples prepared at different times, we obtained the adhesion curves reproducibly at least three times by the measurements for each sample. The most difficulties in the experiments were in the sample preparation rather than the measurement itself. We must carefully handle the sample in order not to risk unnecessary damage to the gel surface. Moreover, the experiments should be conducted quickly to prevent from dehydration. If the several technical conditions were satisfied, however, the absolute values of F_A and E_A were very reproducible within 5% of error bars in the same sample, which was independent of the sampling region.

ATR FTIR measurements and analysis

To study the network structure in the vicinity of the surface, the measurements of Fourier transform infrared (FTIR) spectroscopy with an attenuated total reflection (ATR) method were carried out. ATR FTIR spectra were recorded on an FTIR spectrophotometer (Jasco FTIR610) equipped with an ATR attachment with a horizontal ZnSe crystal (Jasco PRO400S). The resolution of the spectra was 4 cm^{-1}, and scans were repeated 100 times. The depth of penetration of the evanescent wave with the refractive index of 1.4 at 1500 cm^{-1} is estimated to be 0.9 μm when the angle of incidence is 50°. All measurements were performed at ambient temperature (∼ 25°C). To distinguish characteristic bands of the sample gels, all spectra in the experiment were obtained by subtracting the solvent component measured under the same condition. The complex absorption bands obtained here were resolved applying a well established curve fitting method. The second derivatives of spectra of all samples were calculated in the whole range of wave number (1800–1100 cm^{-1}). The components of the absorption band at 1750–1690 cm^{-1} were deduced from these second derivatives, and the curve fittings were conducted using these second derivatives as the initial parameters. The baseline determined from the spectra in the whole range of wave number was used from the respective fitting of the absorption bands and the band shape was analyzed using the mixed Gaussian-Lorentzian function. The wave number, height, and width of the components were optimized to obtain the bestfit curve by an iterative procedure. Analysis of the IR spectra (the subtraction of a water spectrum, the calculation of a second derivative spectrum, baseline subtraction, and curvefitting analysis of complex absorption bands) were performed by using the Spectra Manager software equipped in the spectrophotometer (Jasco).

The IR absorbance spectra were normalized based on CH_2 bending vibration that appears at ∼ 1470–1430 cm^{-1}. The components of the absorption band at 1550–1380 cm^{-1} were deduced from the second derivative of spectra and were resolved applying the curve fitting method. All spectra were found to involve CH_2 bending vibration consisting of two peaks at ca. 1463 cm^{-1} (1464 and 1446 cm^{-1}). The total absorbance areas of the two peaks were assumed to be equivalent in the present experimental conditions, and the spectra were normalized by the total area.

RESULTS

Effects of the normal weight for the separation on F_A and E_A

Figure 3(a,b) shows the W-dependence of F_A and E_A in the log-log scale, which was calculated from the adhesion curves measured under different Ws (two parameters were fixed, $t_w = 60$ s and $v = 1.0$ mm/s). In this figure, W after a slight relaxation (at P_3 in Fig. 2) was used. Although the contact area increased even after the stop of the stage, the change in W was small enough for the present discussion, since the gels were mostly deformed during the approaching process (between P_1 and P_2 in Fig. 2). Both F_A and E_A increased with W, and the W-dependence was approximated by a power law. With increasing x in PSA-Al(x), the absolute values of F_A and E_A at the same W tended to decrease monotonically, while the slope showed a peak at $x = 2$ and rapidly decreased above $x = 2$ [Fig. 3(c)].

Effects of the waiting period for the separation on F_A and E_A

Figure 4(a,b) show the time (t_W) dependence of F_A and E_A in the log-log scale, which was calculated

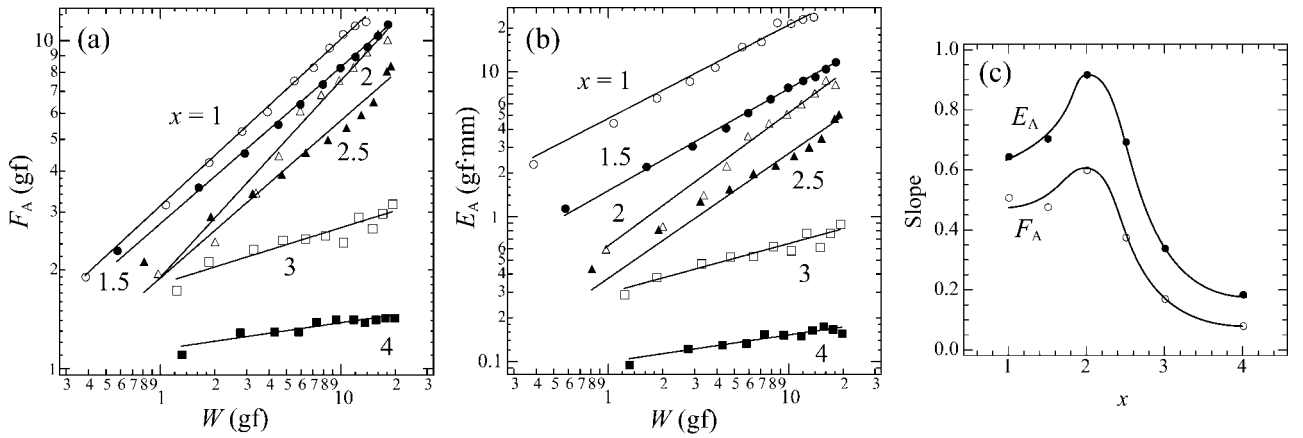

Figure 3 W-dependences of (a) F_A and (b) E_A in log-log scale, which were calculated using the adhesion curves measured under the conditions, t_w = 60 s and v = 1.0 mm/s. The respective solid line was obtained by the least-square method. (c) The slopes are plotted as a function of x in PSA-Al(x).

from the adhesion curves measured under different t_Ws in the range between 1 and 600 s (two parameters were fixed, z_0 = 0.832mm and t_w = 60 s). Both F_A and E_A increased with t_W, and the t_W-dependence was approximated by power laws in the limited range of t_W. Neither F_A nor E_A depended on t_W in the range of t_W larger than 100 s and less than 10 s in the case of $x \leq 1.5$ and $x \geq 3$, respectively. With increasing x, the absolute values of F_A and E_A at the same t_W tended to decrease monotonically, except for F_A of the PSA-Al(1) gel, while the slopes increased at $x = 2$ and almost constant at $x \geq 2$ [Fig. 4(c)]. The exception seen in F_A ($x = 1$) and the small slopes in the case of $x \leq 1.5$ could be understood by the formation of fibrils due to the small bulk modulus (see next section). The elastic modulus was small and the bulk deformation was suppressed by the separation force (see Discussion).

Effects of the receding velocity for the separation on F_A and E_A

Figure 5(a,b) show the v-dependence of F_A and E_A in the log-log scale, which was calculated from the adhesion curves measured under different v's in the range between 0.005 and 10 mm/s (two parameters were fixed, z_0 = 0.832 mm and t_w = 60 s). Both F_A and E_A were found to increase with v, and the v-dependence was approximated by two power laws. With increasing x, the absolute values of F_A and E_A at the same v tended to decrease except for F_A of the PSA-Al(1) gel. The exception seen in F_A (x = 1) could also be understood by the small elastic modulus. All slopes seemed to change at around 0.5 mm/s (between 0.1 and 1 mm/s) with increasing x, while the respective slope before and after the transition did not apparently depend on x [Fig. 5(c)].

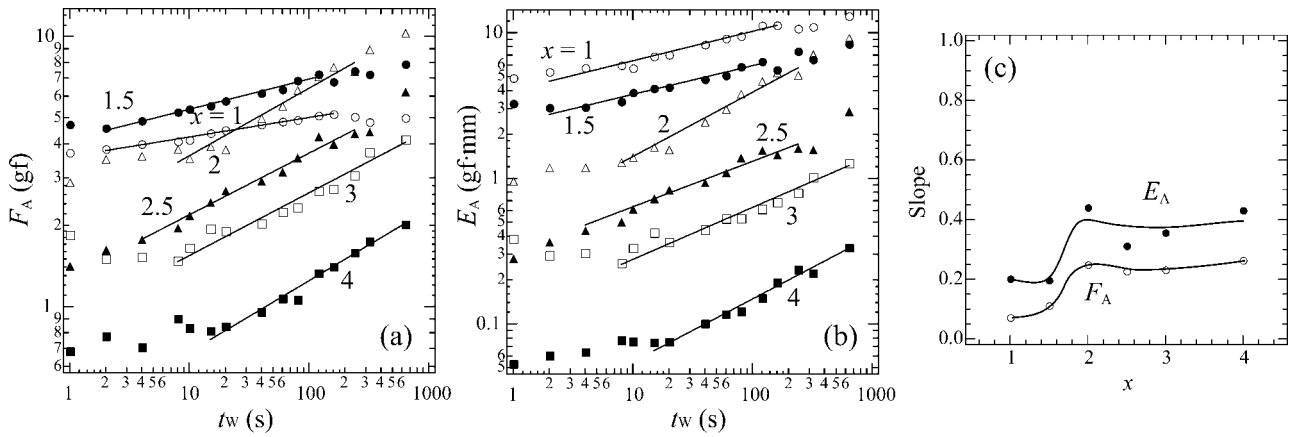

Figure 4 t_w-dependences of F_A (a) and E_A (b) in log-log scale, which were calculated using the adhesion curves measured under the conditions, z_0 = 0.832 mm and v = 1.0 mm/s. The respective solid line was obtained by the least-square method. (c) The slopes are plotted as a function of x in PSA-Al(x).

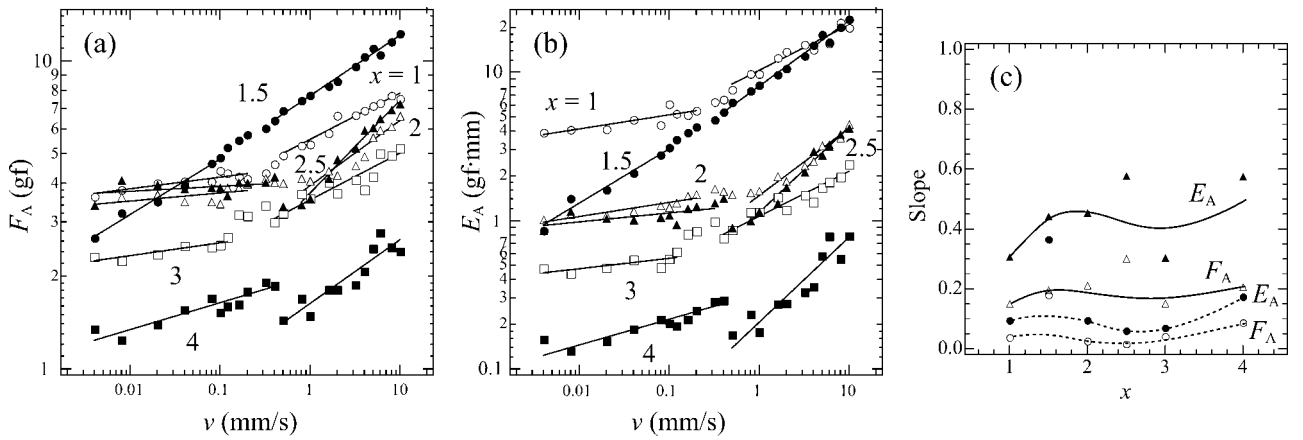

Figure 5 v-dependences of F_A (a) and E_A (b) in log-log scale, which were calculated using the adhesion curves measured under the conditions, z_0 = 0.832 mm and t_w = 60 s. The respective solid line was obtained by the least-square method. (c) The slopes are plotted as a function of x in PSA-Al(x).

ATR FTIR and dynamic viscoelastic measurements

Figure 6a shows the ATR FTIR spectra of the PSA-Al(x) gel (x = 1, 2, 3, and 4). As is shown in this figure, the overall features of the spectra were same and two strong absorption peaks were observed at around 1550 and 1410 cm^{-1}, which did not strongly depend on x. These peaks were assigned to the C=O stretching vibration of the ionized carboxyl group ($—COO^-$). On the other hand, the broad absorption peaks at 1750–1650 cm^{-1} and 1380–1150 cm^{-1}, which seemed to consist of multiple components, decreased monotonically with increasing x. This evidence indicated that the degree of crosslinking might affect the intermolecular force between the carboxyl groups and Al ions in a monotonic fashion with increasing x. To investigate the formation of hydrogen bonds in detail, a curve-fitting analysis of the nonionized carboxyl region (1800–1500 cm^{-1}) was performed by the deconvolution of the spectra. From the results of the second-derivative spectra, there were four peaks (at around 1746, 1731, 1716, and 1697 cm^{-1}) that were reproducible in this region due to the C=O band of the nonionized carboxyl groups. According to the literature,[20–24] the peak located at around 1748 and 1738 cm^{-1} can be assigned to the C=O stretching vibration of the free (non-hydrogen-bonded) carboxyl groups (free C=O), and the peak located at around 1716 and 1700 cm^{-1} can be assigned to the C=O stretching vibration of the hydrogen-bonded carboxyl groups in a dimeric form (C=O···H—O hydrogen-bond). Figure 6(b) shows the peak areas of the respective sum of two components. The data presented in this figure show that both numbers of non-hydrogen-bonded and hydrogen-bonded carboxyl groups tended to decrease with increasing x. In addition, the broad peak at 1350–1200 cm^{-1} slightly but evidently

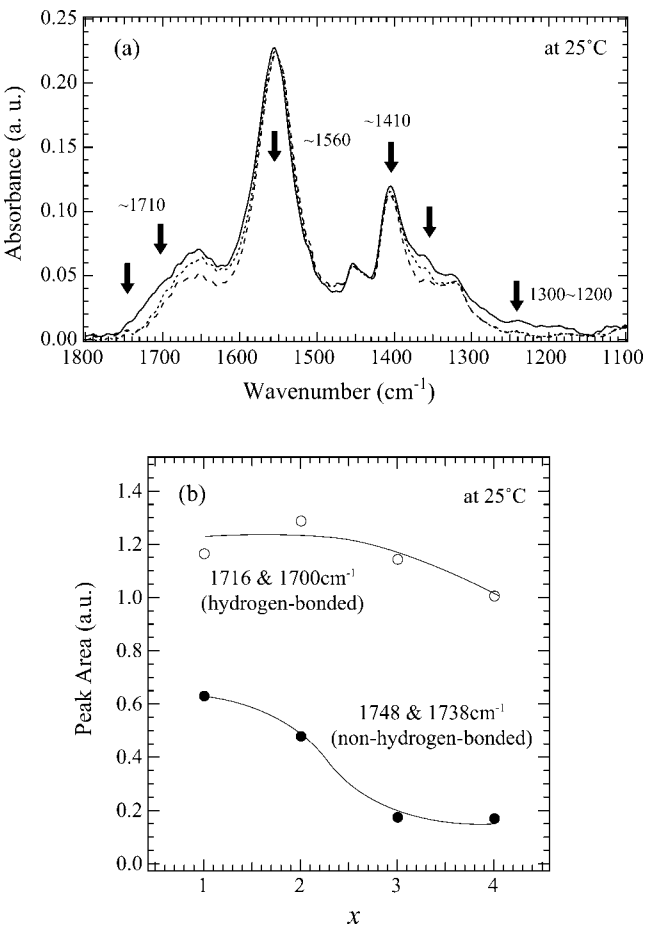

Figure 6 (a) ATR FT-IR spectra of PSA-Al(x) gel (x = 1, 2, 3, and 4) at 25°C. (b) Peak area ratios of the C=O stretching vibrations, resulting from the two origins; the free (non-hydrogen-bonded) carboxyl groups at around 1748 and 1738 cm^{-1}, and the hydrogen-bonded carboxyl groups at around 1716 and 1700 cm^{-1}. Each area denotes the sum of the respective two components. The solid lines were added to guide the eye.

decreased with increasing x. This broad peak could be assigned to the coupled peaks of the C=O stretching vibration and the O—H bending vibration in the cyclic hydrogen bonds between two carboxyl groups.[20] Therefore, with increasing x the number of nonionized carboxyl groups (—COOH) decreased, while the number of ionized carboxyl groups ($—COO^-$) was unchanged.

To investigate the bulk stiffness, the measurements of the dynamic shear viscoelasticity were conducted at a frequency range between 0.05 and 3 Hz using a rheometer (UBM; MR300) equipped with a parallel plate geometry. As is shown in Figure 7, the viscoelastic behavior of the aqueous PSA solutions was completely different from those of PSA-Al(x) gels (x = 1, 1.5, 2, 2.5, 3, and 4). In the cases of gels, the storage modulus G' was larger than the loss modulus, G', showing that the elastic characteristic has a principal role in the gel structure. The storage modulus, G' increased with time and became independent of the frequency after the gelation, in agreement with the existence of a network structure. On the other hand, the G' value of PSA-Al(x) gels increased as a function of x, suggesting an increase of the number of crosslinking; Al ions were expected to be complexed with the carboxyl groups on PSA. The stiffness increased with increasing x; more precisely it increased rapidly and slowly below and above x = 2.5, respectively. The G' values were highly correlated with x (Al content), and they tended to saturate above x = 2.5. In conjunction with this observation, it is noteworthy that G'' started to decrease within the frequency range measured here when x exceeded 2. Although the frequency of the present experiment was limited, this behavior suggested the shift of the peak frequency of G'' to the lower range, which was attributed to the decrement of viscosity with time.

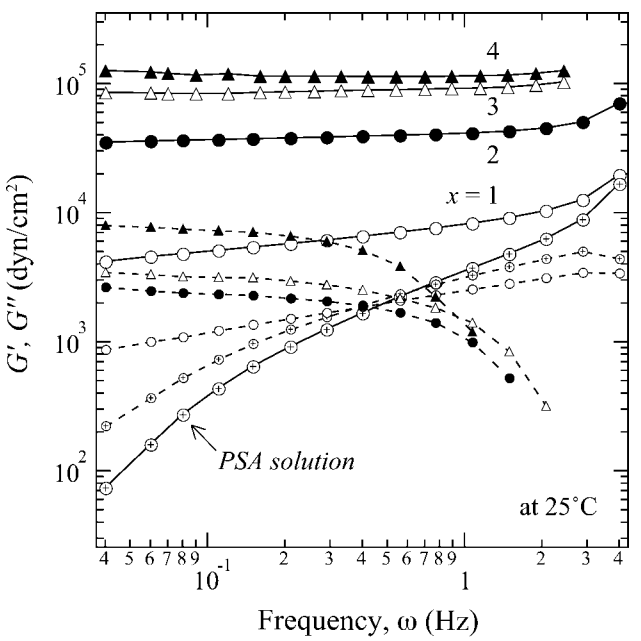

Figure 7 Shear storage modulus, G' (larger symbols and solid lines) and G'' (smaller symbols and broken lines; each symbol corresponds to the respective one of G') of the aqueous PSA solution and PSA-Al(x) gel (x = 1, 1.5, 2, 2.5, 3, and 4), which were measured using a rheometer with a parallel plate geometry. In the gelation process, G' increased with time, and it became independent on the frequency. The G' values were highly correlated with x (Al content), and they tended to saturate above x = 2.5.

DISCUSSION

Power-law behavior of F_A and E_A depending on the experimental conditions

Among the present findings, the observation of the power-law behavior of F_A and E_A against the experimental conditions (W, t_W, and v) seemed highly specific to the crosslinked polymeric soft materials. The number of powers that can be seen, more than one for t_W and v, as well as the absolute values of F_A and E_A, depended on x. These findings could be related with the interfacial adhesion (surface physical and chemical properties) and the bulk elastic properties. The roles of the interfacial and bulk properties in determining the adhesion properties should depend on the material parameters as well as the experimental conditions.

On the basis of the dependences of three parameters on F_A and E_A, we can infer the origins of adhesive interactions at the molecular scale. It is reasonable to suppose that the surface of gels consisted of a large number of asperities,[25,26] which originated in the micro-domains introduced at gelation.[27,28] Therefore, the true contact area, S_T could be expected to be different from the apparent contact area, S. In the nanoscopic level, each asperity consisted of polymer chains; the true contact area was made of a large number of small regions that formed asperities, where the molecular-to-molecular contacts in polymer chains[29,30] took place, as is shown in Figure 8. Therefore, the deformation of the asperities might increase S_T (the number of interactions in the molecular scale), and F_A and E_A could be determined by S_T, which might be affected by the experimental conditions (W, t_W, and v). Therefore, the present results could be discussed on the basis of the balance between the apparent contact (the number of asperities) and the asperity contact (the true contact area).

In the case of W-dependence, F_A and E_A were simply approximated by a single power law [Fig. 3(a,b)], indicating a single mechanism of the separation in the whole W range used in the present measurements. We believe that the power-law behavior observed in the present samples resulted from two specific factors; one was the macroscopic deforma-

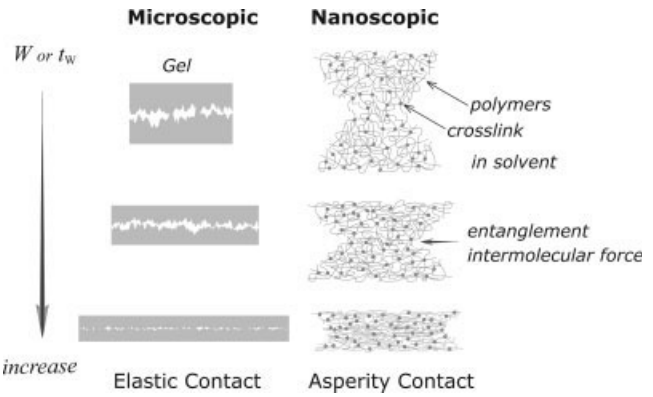

Figure 8 Schematic representation of the multi-scale contacts in the microscopic and nanoscopic levels. Each size is related with the contact of the micrometer domains and the nanometer domains (minimum unit of contact). In the nanometer scale, the molecular-to-molecular contacts, including entanglements and the intermolecular force, are essential in determining the adhesion properties.

tion of gels caused by W, which increased the apparent contact area, and the other was the microscopic deformation of asperities, which increased S_T. The single power indicated that the normal force cooperatively increased S_T by increasing the number of asperity contacts as well as the deformation of the asperities. In the case of t_W-dependence, F_A and E_A were approximated by a single power law in the middle-t_W range of the present measurements [Fig. 4(a,b)], which could result from the same origin as the W-dependence. Although F_A and E_A deviated from the power law in the low-t_W range (and in the high-t_W range for small x), the overall feature was the same as the W-dependence.

In the case of v-dependence, on the other hand, it was interesting to observe that F_A and E_A were approximated by two power laws below and above a specific v [Fig. 5(a,b)], indicating two different mechanisms of separation. The respective specific v was between 0.1 and 1 mm/s, which might not depend on x. According to the peeling test on adhesive tapes, the existence of two states against the peel speed has been reported[31,32]; at a lower peel speed, the large deformation of the peeled adhesive causes energy dissipation (viscous peeling), and at a higher speed, adhesive failure occurs before large deformation of the peeled adhesive (elastic peeling). This transition from the viscous to the elastic property is the most likely reason for the present observation of two power laws in this case of v-dependence.

Effects of the surface and bulk properties depending on the material parameters

To understand the effects of the macroscopic deformation of gels on the adhesion properties, the material parameters were examined on the basis of the present results. The increment of F_A should be determined by the increment of the apparent contact area, S, since the contact number of the microdomains in the mesoscopic level should increase with increasing the macroscopic deformation of gels. In general, the determination of S for an adhesion test provides critical information, especially for proper interpretation of the bulk and interfacial contributions to adhesion. Although the direct *in situ* measurements of S were in principle difficult in the present experimental situations, we developed an indirect measurements and obtained a rough estimation of S (the stamp experiment); a vermilion ink (made of vegetable oil, synthetic resin, and pigment) was spread on one of the samples before the contact and its imprint in the other sample was obtained after the separation. As is shown in Figure 9, the imprint was a white circle with a dark circumference (the color was red); the white part was a contact area and the dark one resulted from the diffusion of vermilion ink, which was squeezed out from the contact area. For PSA-Al(x) gels (x = 2 and 3), we measured the diameter of the white circle and calculated the directly measured contact area, S_0. Figure 10(a) shows the W-dependence of S_0 together with the displacement by a contact along the z-direction, Δh, which was obtained from the adhesion curve (Fig. 2) measured simultaneously in the stamp experiment. As a result,

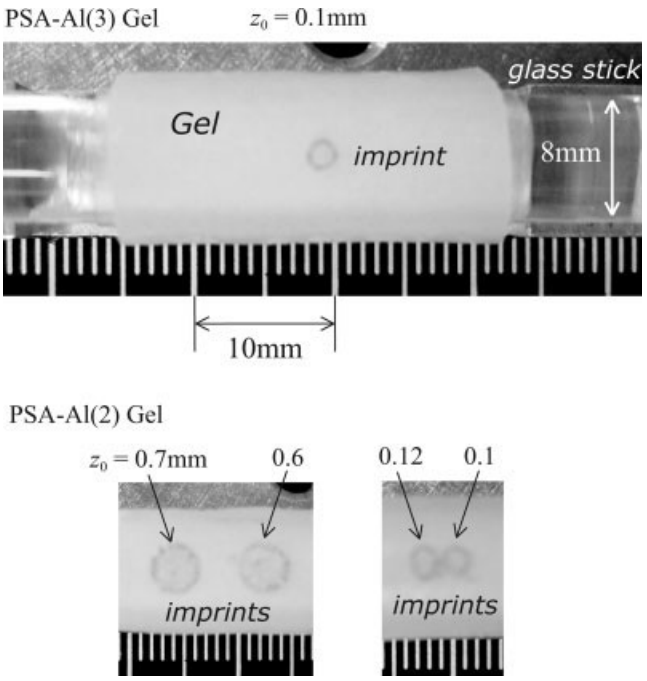

Figure 9 Examples of imprint obtained by the stamp experiment in PSA-Al(3) gel under the conditions, z_0 = 0.1 mm, t_w = 60 s, and v_0 = v = 1.0 mm/s; the area of the white circle was 1.1 mm^2 (top). Change in the imprint with increasing z_0 is shown in the cese of PSA-Al(2) gel.

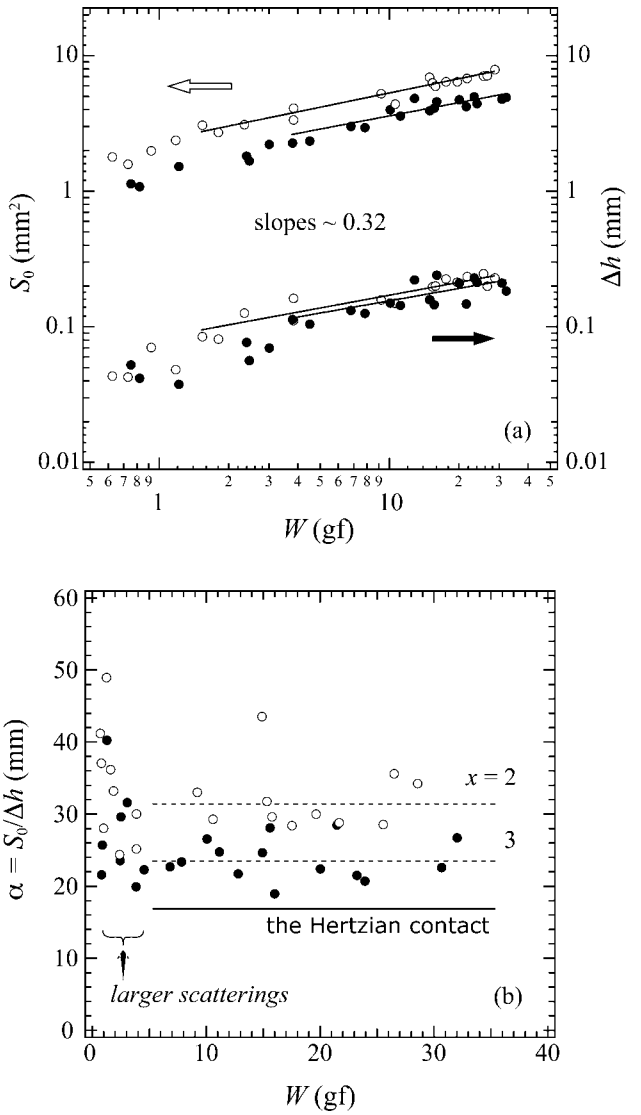

Figure 10 (a) W-dependences of the directly measured contact area, S_0 obtained by the stamp experiment and the displacement by a contact along the z-direction, Δh obtained from the adhesion curve. The respective solid line was obtained by the least-square method. (b) W-dependences of $S_0/\Delta h$.

the slopes of the W-dependence of S_0 was approximately 0.32 ($\pm$0.02), which was much smaller than the expected value of 2/3 for the Hertzian contact, but almost same as the slope of the W-dependence of Δh. As is shown in Figure 10(b), $S_0/\Delta h$ was roughly constant except in the small range of W; $S_0 = \alpha\Delta h$. The average of α depended on x (α = 31.5 for x = 2 and 23.6 for x = 3) and it was evidently larger than 17.6 (= πR_0; the curvature of the top surface of gel, R_0 = 5.6 in the present experiments), which is predicted by the Hertzian contact ($S = \pi R_0 \Delta h$).[11,15]

With decreasing W, Δh is expected to approach zero and it can be negligibly smaller than the gel thickness, which suggests that α approaches 17.6. The experimental results, however, indicated that α showed a larger scattering and tended to increase with decreasing W. The most possible reasons to explain the deviation from the prediction should be an adhesive force between gel surfaces, the capillary effects at the circumference, and the pore pressure effects of water during the network deformation. These effects should be taken into consideration since the measurements were conducted in the air under dynamic loading conditions (t_w (= 60 s) was too small for the gels to be equilibrium). The relation between S and Δh in the small range of W is an important subject for future investigations.

Although the real effective factors in determining S was much more complicated than these considerations, the stamp experiment indicated that S_0 was proportional to Δh except in the small range of W and larger than the predicted one by the Hertzian contact. On the basis of this finding, we evaluated the effects of the apparent contact area on the W- and t_W-dependences; F_A and E_A (in Figs. 3 and 4) were divided by S_0 (= $\alpha\Delta h$), where Δh was obtained in the respective adhesion experiment and α was obtained in the stamp experiment (separately conducted). As is shown in Figure 11, the W- and t_W-dependences of F_A/S_0 and E_A/S_0 in the log-log scale was characterized not only by the overall absolute values but also by the approximation of power laws with multiple slopes. The absolute values of PSA-Al(2) were larger than those of PSA-Al(3) in both the W- and t_W-dependences. This observation could be attributed to the facts that the non-hydrogen-bonded carboxyl groups decreased [Fig. 6(b)] and the bulk elasticity increased (Fig. 7) with increasing x. These two factors of the surface and bulk corresponded to the decrease of interfacial adhesion and the increase of the bulk elastic properties, respectively.

As for the multiple slopes, the signs of slopes, i.e., minus, zero, and plus (corresponding to a decrement, a constant, and an increment of F_A and E_A, respectively) could be seen in Figure 11. In the case of the W-dependence, it is interesting to observe that F_A/S_0 and E_A/S_0 of PSA-Al(3) decreased and became constant with increasing W, while those of PSA-Al(2) increased when W exceeded around 3 gf. We believe that this complicated power law behavior, which depended on x, could be attributed to the deformation of asperities, which could not linearly increase with increasing the apparent contact area by the bulk deformation. The negative slope appeared in the case of PSA-Al(3) was understandable from Figure 3(c), where the slope of F_A or E_A versus W was smaller than that of S_0 versus W [approximately 0.32 in Fig. 10(a)]. The negative slope suggested that the increase rate of the true contact area was smaller than that of the apparent contact area, in other words, the deformation rate of the asperities was smaller than that of the bulk deformation. We

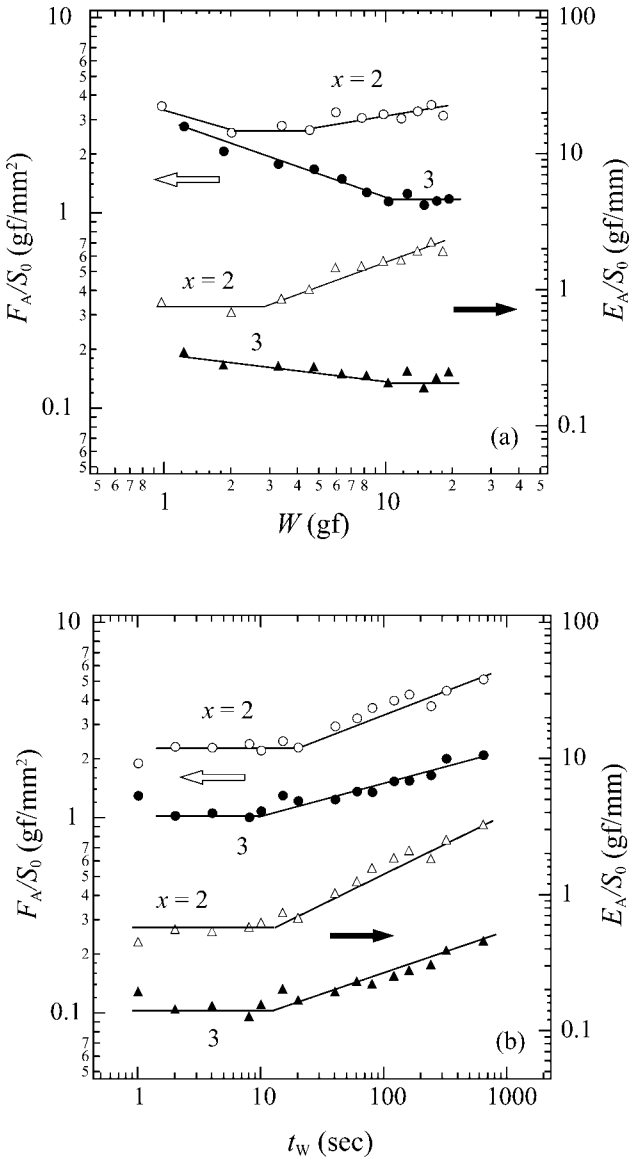

Figure 11 Adhesion force and energy per unit contact area, F_A/S_0 and E_A/S_0, as functions of (a) W and (b) t_w. The solid lines were added to guide the eye. Each curve consists of multiple components.

assume that the stiffness of the asperities is apparently larger than that of the bulk, which might result from the slight dehydration of the surface by contact with the air (the experiments were conducted in the air). On this assumption, the difference between the surface and bulk mechanical properties might be the most likely reason for the existence of negative slope.

In the case of t_W-dependence, on the other hand, the negative slope was missing, and the dependences of F_A or E_A and F_A/S_0 or E_A/S_0 against t_W were almost identical [compare Fig. 4(b) with Fig. 11(b)]. Considering that the slopes of the t_W-dependence of S_0 were comparable to those of F_A and E_A, this observation indicated that the deformation rate of the asperities was almost same as the increase rate of the number of asperity contacts. In the context of the discussion of the deformation of the asperities, however, the origin of the t_W-dependence should be the same as that of the W-dependence. We believe that the absence of negative slope in the t_W-dependence could be attributed to the relatively large W used in the measurements of the t_W-dependence (under $z_0 = 0.832$ mm that produced a 10 gf restoring force by the present spring distortion); the negative slope could be seen uder a small W.

Although we do not have a quantitative model to explain the picture of the negative slope, there are two noteworthy properties in the small range of W. One is that S_0 was underestimated due to the aforementioned effects of adhesive force and capillary force. The other is that the thickness may change during the measurements due to the dehydration. Although the thickness change due to the dehydration was small during the measurements, it should affect the adhesive properties in the top surfaces to some extent. According to our previous work,[19] the inhomogeneous network in as-synthesized PSA gels consists of dilute or dense area of polymer density, which might be enhanced during the dehydration. If the minute physical and chemical properties of these effects were to be examined, the negative slope could be explained. This is an important subject for future investigations.

Finally, the formation and annihilation of fibrils resulting from the flow of the polymers near the surfaces in the cases of small x are noteworthy. In the case of the weaker gel ($x \leq 1$), the macroscopic fibrils should have important roles in determining the adhesion properties rather than the bulk deformation. On the other hand, the bulk stiffness could be ignored for highly crosslinked gels, where the interfacial adhesion became essential. The balance between the contributions from interface and bulk could determine the adhesion properties in the present system. To control the adhesion of soft materials, optimization of the experimental conditions as well as the material parameters are required. Experiments on not only the microscopic but also nanoscopic studies of polymer gel surfaces are important subjects for future investigations.

CONCLUSIONS

The adhesion properties of swollen PSA hydrogels physically crosslinked by aluminum ions were evaluated by a point-contact method in the air at room temperature. As a result, F_A and E_A increased with increasing the experimental conditions (W, t_W, and v) and obeyed power laws. With increasing the degrees of the crosslinking, the absolute values of F_A and E_A tended to decrease monotonically.

The contact area was directly measured, which was proportional to the deformation by a contact along the normal direction to the surface except in the small range of W. The measurements of ATR FT-IR spectroscopy were conducted, which demonstrated that the degree of crosslinking affected the intermolecular force between the carboxyl groups and Al ions; the number of nonionized carboxyl groups (—COOH) decreased with increasing the degree of crosslinking. The measurements of the dynamic shear viscoelasticity were also conducted and the stiffness increased and tended to saturate with increasing the degree of crosslinking. From these additional experiments, the experimental results were qualitatively understood on the basis of the balance between the interfacial adhesion (surface physical and chemical properties) and the bulk elastic properties; F_A and E_A were determined not only by the interfacial adhesion but also by the bulk elastic properties.

The present observations, we believe, are of crucial importance not only when designing the adhesion force and separation energy of swollen hydrogels in general but also for developing the foundation for future practical applications of hydrogels as functional elements. In such a further investigation, the present technique can be widely applicable for weakly adhering soft materials like swollen hydrogels with relative high accuracy and reproducibility.

References

1. Shull, K. R. Mater Sci Eng Rep 2002, 36, 1.
2. Webber, R. E.; Shull, K. R.; Roos, A.; Creton, C. Phys Rev E 2003, 68, 021805.
3. Gent, A. N. Langmuir 1996, 12, 4492.
4. Mizumachi, H. J Appl Polym Sci 1985, 30, 2675.
5. JIS Z 0237, Testing Methods of Pressure Sensitive Adhesive Tapes and Sheets, Japan, 1991.
6. Asahara, J.; Hori, N.; Takemura, A.; Ono, H. J Appl Polym Sci 2003, 87, 1493.
7. PSTC-6 Tack Rolling Ball, Adhesion Test Methods, Test Methods for Pressure Sensitive Adhesive Tapes, 15th ed.
8. ASTM D3121. Standard Test Method for Tack of Pressure-Sensitive Adhesives by Rolling Ball, 1999.
9. Urahama, Y. J Adhes 1989, 31, 47.
10. Sato, T.; Goto, M.; Nakano, K.; Suzuki, A. Jpn J Appl Phys 2005, 44, 8168.
11. Hertz, H. J Reine Angew Math 1882, 92, 156.
12. Johnson, K. L.; Kendall, K.; Roberts, A. D. Proc R Soc London Ser A 1971, 324, 301.
13. Derjaguin, B. V.; Muller, V. M.; Toprov, Y. P. J Colloid Interface Sci 1975, 67, 314.
14. Maugis, D.; Pollock, H. M. Acta Metall 1984, 32, 1323.
15. Johnson, K. L. Contact Mechanics; Cambridge University Press: Cambridge, UK, 1985.
16. Silberzan, P.; Perutz, S.; Kramer, E. J.; Chaudhury, M. K. Langmuir 1994, 10, 2466.
17. Chaudhury, M. K. Mater Sci Eng Rep 1996, 16, 97.
18. Tamagawa, H.; Nogata, F.; Umemoto, S.; Okui, N.; Popovic, S.; Taya, M. Bull Chem Soc Jpn 2002, 75, 383.
19. Harada, T.; Hirashima, Y.; Suzuki, A.; Goto, M.; Kawamura, N.; Tokita, M. Eur Polym J 2005, 41, 2189.
20. Sato, H.; Hirashima, Y.; Suzuki, A.; Goto, M; Tokita, M. J Polym Sci Part B: Polym Phys 2005, 43, 753.
21. Hirashima, Y.; Sato, H.; Suzuki, A. Macromolecules 2005, 38, 9280.
22. Maeda, M.; Yamamoto, H.; Ikeda, I. Langmuir 2000, 16, 7503.
23. Maeda, M.; Higuchi, T.; Ikeda, I. Langumuir 2001, 17, 7535.
24. Dong, J.; Ozaki, Y.; Nakashima, K. Macromolecules 1997, 30, 1111.
25. Biggs, S.; Spinks, G. J Adhes Sci Technol 1998, 12, 461.
26. Rabinovich, Y. I.; Adler, J. J.; Ata, A.; Singh, R. K.; Moudgil, B. M. J Colloid Interface Sci 2000, 232, 10.
27. Suzuki, A.; Yamazaki, M.; Kobiki, Y. J Chem Phys 1996, 104, 1751.
28. Suzuki, A.; Yamazaki, M.; Kobiki, Y.; Suzuki, H. Macromolecules 1997, 30, 2350.
29. Maeda, N.; Chen, N.; Tirrell, M.; Israelachvili, J. N. Science 2002, 297, 379.
30. Allegra, G.; Raos, G. J Chem Phys 2006, 124, 144713.
31. Nasuno, S.; Kudrolli, A.; Bak, A.; Gollub, J. P. Phys Rev E 1998, 58, 2161.
32. Yamazaki, Y.; Toda, A. J Phys Soc Jpn 2004, 73, 2342.